Electrochimica Acta 176 (2015) 982–988

Contents lists available at ScienceDirect

Electrochimica Acta

journal homepage: www.elsevier.com/locate/electacta

Nitrogen, oxygen and phosphorus decorated porous carbons derived from shrimp shells for supercapacitors

Jiangying Qu[a,*], Chuang Geng[a], Siyuan Lv[a], Guanghua Shao[a], Shiyao Ma[a], Mingbo Wu[b,**]

[a] Faculty of Chemistry and Chemical Engineering, Liaoning Normal University, Dalian, Liaoning 116029, China
[b] State Key Laboratory of Heavy Oil Processing, China University of Petroleum, Qingdao 266580, China

ARTICLE INFO

Article history:
Received 2 February 2015
Received in revised form 16 July 2015
Accepted 17 July 2015
Available online 26 July 2015

Keywords:
porous carbon
heteroatom doping
biomass
shrimp shell
supercapacitor

ABSTRACT

Nitrogen (N), oxygen (O) and phosphorus (P) decorated porous carbon (PC) is *in situ* synthesized for supercapacitors by H_3PO_4 activation of shrimp shell. The results show that shrimp shell with 5.32 wt% nitrogen, 30.1 wt% carbon and 40.2 wt% oxygen is a good carbon precursor, and H_3PO_4 plays an important role on the formation of porous structure and P doping. The contents of N, O and P functional groups in the resultant carbons along with their porosities are temperature-dependent. PCs with abundant pores and heteroatom functionalities are good electrode materials for supercapacitors in basic medium. Typically, PC with moderate N, O and P contents, large surface area and co-existence of mesopores with micropors exhibits a high specific capacitance of 206 F g^{-1} at 0.1 A g^{-1} in 6 M KOH solution. Furthermore, the energy density and power density of obtained PC electrodes can be substantially improved by widening the operation voltage window with the assistance of doped P. Specifically, its energy density can increase greatly from 2.9 Wh kg^{-1} at 0.9 V to 5.2 Wh kg^{-1} at 1.1 V. The present study demonstrates a feasible and effective strategy to develop high-performance supercapacitors economically from waste biomass and also helps to understand the roles of heteroatom on the electrochemical performances of PC electrodes.

1. Introduction

Supercapacitors have attracted great attention owing to their high rate capability, long cycle life, large power density and low maintenance [1,2]. Based on the different charge-storage mechanisms, supercapacitors can be divided into two categories: one is the electrical double-layer capacitors (EDLCs), as characterized by high power density and long cycle life, in which the capacity arises from the electrosorption of ions on porous carbon (PC) electrodes at the electrode/electrolyte interface [3–6]. The other is the pseudocapacitors with high energy density but poor power density and cycle stability, its capacity comes from faradaic reactions at the electrode/electrolyte surface [3–7]. The electrode materials are the key components determining their capacitance performance, and PCs are the most reported electrode materials owing to their large surface area, tunable pore structure and good electrical conductivity [8–11]. Many strategies have been carried for optimizing the energy density of capacitors while keeping a high power density for supercapacitors [12,13], and pseudocapacitance materials are important candidates in this respect. Surface-functionalized carbon materials containing heteroatoms such as nitrogen or oxygen exhibit pseudacapacitance due to charge or mass transfer between the electrode and the ions of the electrolyte [14,15]. It is known that oxygen functionalities are usually present on the surface of PC as a residue from the carbon source or a result of activation process. The pseudocapacitance contribution of nitrogen to the capacitance of PC has also been widely reported [16]. Various techniques have been focus on the introduction of nitrogen species into the carbon framework, which is achieved either by using nitrogen-containing precursors such as melamine and polyvinylpyridine or via treating carbon materials with ammonia gas [17–19]. Despite the great efforts on synthesis of nitrogen-doped carbon electrodes with high capacitive performance, the exploration of renewable biomass with lots of heteroatom as raw material to produce electrode materials would be more worthwhile considering the potential scale of supercapacitor applications [20].

Shrimp shell, a kind of food waste in high quantity, is a cheap and reliable biomass source without increasing competition for

* Corresponding author. Tel.: +86-411-82158329.
** Corresponding author. Tel.: +86-532-86983452.
E-mail addresses: qujy@lnnu.edu.cn (J. Qu), wumb@upc.edu.cn (M. Wu).

http://dx.doi.org/10.1016/j.electacta.2015.07.094
0013-4686/

food. Shrimp shell is composed of nitrogen containing polysaccharide named as chitin (poly-b(1/4)-N-acetyl-D-glucosamine), which can be used as the precursor to directly produce nitrogen doped carbons by pyrolysis technique [21]. However, such carbons usually have poor capacitance when used as the supercapacitor electrode because of their relatively low porosity. Usually, physical or chemical activation of carbon precursors can be used to introduce pores into the resultant carbons, allowing good performance as electrodes for supercapacitors due to the synergistic effect of EDLCs and pseudocapacitors [22,23]. Herein, we report a simple, sustainable preparation of nitrogen/oxygen/phosphorus (N/O/P) heteroatom decorated PCs via *in-situ* H_3PO_4 activation of shrimp shell. Following two advantages brought by H_3PO_4 as the activating agent can be actualized: (1) Porous structures can be introduced into the carbon materials, thus improve the power density of supercapacitors. (2) Phosphorus atom can be in situ introduced into the carbon framework, which can improve its energy density. As expected, the resultant PCs exhibit good electrochemical performances when used as supercapacitor electrodes.

2. Experimental

2.1. Synthesis of N/O/P decorated PCs from shrimp shell

After being cooked and eaten, Bohai shrimp shell was used as the raw material in this study. The shell was sufficiently dissolved in 10 wt% HCl solution at room temperature until the complete removal of $CaCO_3$, then recovered by filtration and washed abundantly with distilled water and dried at 80 °C for 4 h. Activation process was performed as follows. Firstly, above treated shell and phosphoric acid (H_3PO_4, 85 wt%) with a weight ratio of 1:3 were thoroughly mixed together and dried at 80 °C overnight. Then the dried mixture was calcinated at 400∼600 °C for 1 h in a horizontal furnace in Ar. Finally, the samples were thoroughly washed by several cycles of rinse-centrifugation with boiling water until the solution became neutral. After exposure in oven at 80 °C, a series of samples were harvested and denoted as H_3PO_4/C-T (T = 400, 500 or 600 °C). For comparison, C-500 was synthesized in the absence of H_3PO_4 at 500 °C by a similar procedure.

2.2. Electrochemical Measurements

The electrochemical properties of as-obtained samples were investigated using a three-electrode cell and a two-electode cell at room temperature. The working electrodes were fabricated by mixing the prepared powders with 10 wt% acetylene black and 5 wt% polytetrafluoroethylene (PTFE) binder. A small amount of ethanol was added to the mixture to produce a homogeneous paste. The mixture was pressed onto nickel foam current-collectors (1.5 cm in diameter) to make electrodes. The mass of the active material was in a range of 4-5 mg per electrode. Before the electrochemical test, the as-prepared electrode was soaked overnight in a 6 M KOH electrolyte. For the three-electrode cell, platinum foil and Hg/HgO electrode were used as the counter and reference electrodes, respectively. For two-electrode cell, two symmetrical work electrodes were assembled and tested at different cell voltages. The cyclic voltammetry (CV) measurement was conducted on a LK2005A electrochemical workstation (Tianjin Lanlike Company, China), and the galvanostatic charge-discharge measurement was performed on a Land CT2001A cycler at room temperature (Wuhan Land Instrument Company, China). The morphologies and structures of the as-obtained products were examined using field emission scanning electron microscopy (SEM, Hitachi Ltd SU8010), X-ray photoelectron spectroscopy (XPS, Thermo VG Scientific Sigma Probe Spectrometer) and elemental analysis (Elemental Analyzer Vario EL III). The Brunauer-Emmett-Teller (BET) surface area of as-synthesized samples was determined by physisorption of N_2 at 77 K using a Micromeritics ASAP 2020 analyzer.

3. Results and discussion

Fig. 1 illustrates the strategy for the synthesis of N/O/P decorated carbons with porous structures using shrimp shell as the carbon precursor by one-step H_3PO_4 activation. $CaCO_3$ in shrimp shell was firstly removed by HCl, then in situ activated by H_3PO_4 at 400∼600 °C in Ar. PCs with 21-24 wt% of yield were obtained and used as electrode materials for supercapacitors.

Shrimp shell undergoes thermal decomposition and activation by H_3PO_4 during heat treatment, and lots of heteroatoms including N, O and P can still remain in the final PCs. SEM image of H_3PO_4/C-500 sample (Fig. 2a) shows a homogeneous structure sintered after carbonization. Energy-dispersive X-ray Detector (EDX) mapping was performed to study the element distribution of N, O, P decorated PCs (Figs. 2b∼d). Results indicate N, O and P are uniformly distributed in the whole carbon network. EDX analysis exhibits 4.93 at.% N, 13.5 at.% O and 1.75 at.% P existed in H_3PO_4/C-500 sample. FTIR spectra of PCs obtained by H_3PO_4 activation of shrimp shell are shown in Fig. 2e. For C-500 without H_3PO_4 activation, the peaks at 1074, 1400 and 1640 cm^{-1} are respectively attributed to C-O, C-N and N-H stretches [24,25], which come from the decompositions of protein and chitin in shrimp shell. After H_3PO_4 activation under the same condition, new intense peaks besides above mentioned appear in the FTIR spectra of H_3PO_4/C samples. The new peak at 1168 cm^{-1} can be assigned to the stretching vibration of hydrogen-bonded P=O groups in the P-O-C linkage [26]. The results demonstrate that N, O, P functional groups coexist in PCs prepared by H_3PO_4 activation of shrimp shell.

In order to elucidate the surface composition of the carbon electrode and its role in the electrochemical performance of obtained PCs, the incorporated N, O and P are further analyzed by elemental analysis and XPS (Fig. 3), and their quantitative analyses are listed in Table 1. As can be seen from Table 1, N, P, O contents decrease significantly with the temperature increasing from 400 to 600 °C in the presence of H_3PO_4, indicating the N, O, P functionalities in PCs are temperature-dependent. For comparison, C-500 displays 3.44% N and 15.13% O, while H_3PO_4/C-500 shows 3.34% N, 13.11% O and 1.77% P. It is obvious that the H_3PO_4 activation can decorate P into PC from shrimp shell. From the XPS spectra of N1s (Fig. 3a), the most pronounced peaks represent pyridinic N (N-6 at 398.5 eV), pyrrolic/pyridonic N (N-5 at 399.5 eV), quaternary

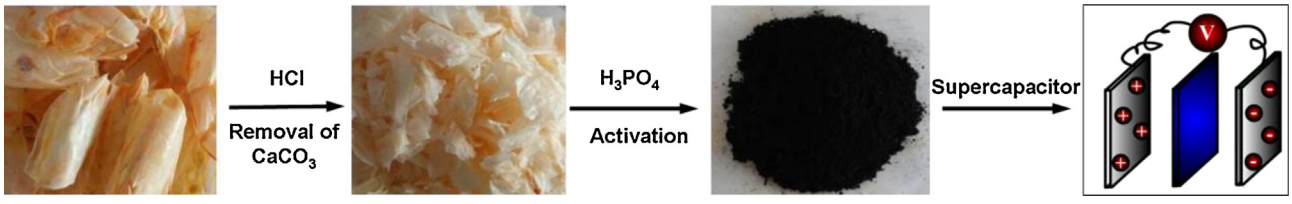

Fig. 1. Synthesis schematic of N/O/P decorated PCs for supercapacitors using shrimp shell as the carbon precursor.

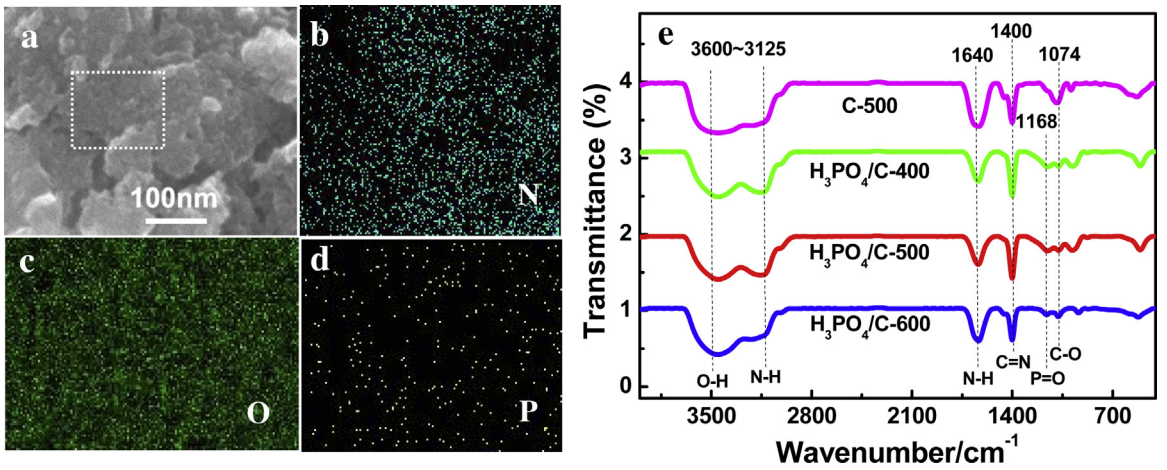

Fig. 2. SEM image (a) and mapping (b, c, d) of H_3PO_4/C-500; (e) FTIR spectra of C-500, H_3PO_4/C-400, H_3PO_4/C-500 and H_3PO_4/C-600 samples.

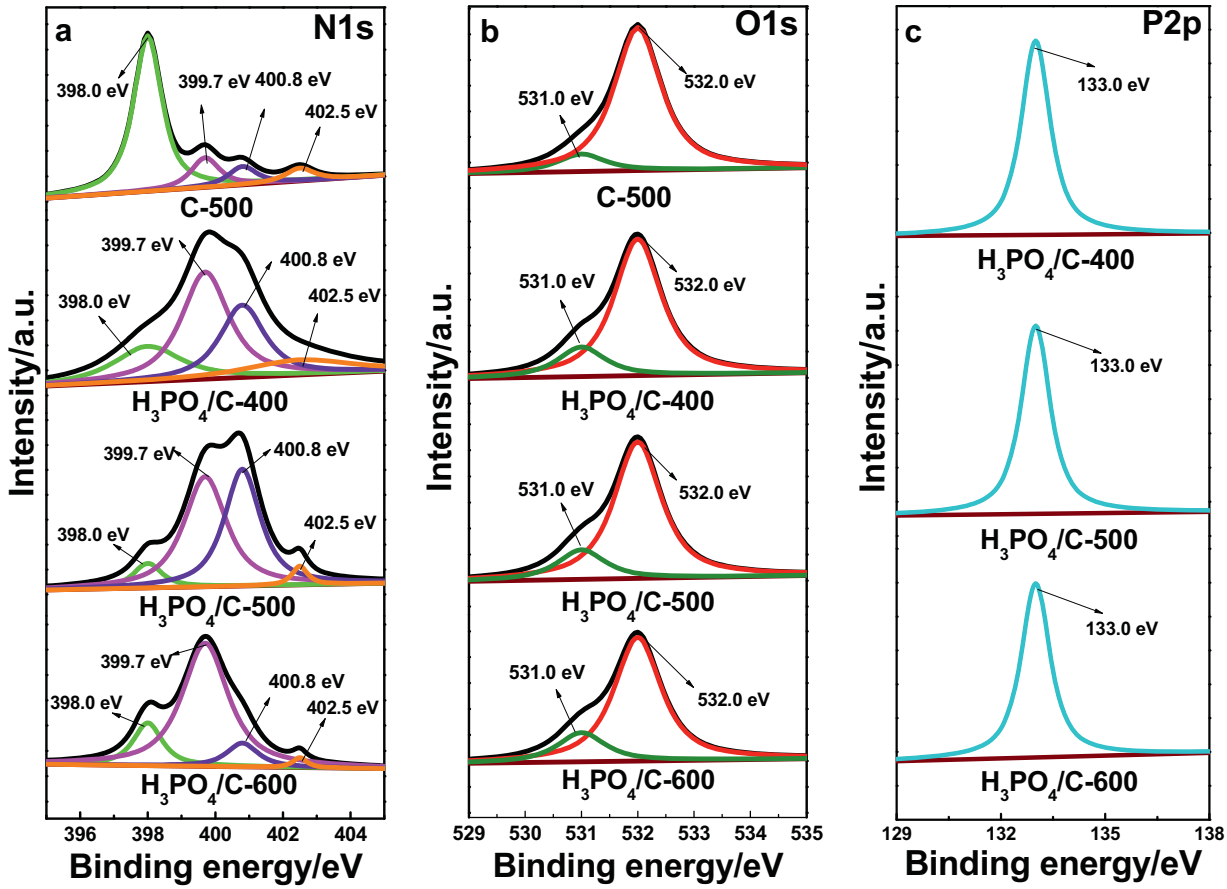

Fig. 3. XPS survey of deconvoluted high-resolution (a) N1s, (b) O1s for C-500, H_3PO_4/C-400, H_3PO_4/C-500 and H_3PO_4/C-600 samples and (c) P2p for H_3PO_4/C-400, H_3PO_4/C-500 and H_3PO_4/C-600 samples.

Table 1
The contents of N, P and O in PCs from elemental analysis and XPS analysis.

	Elemental analysis (at %)			N-6 [%]	N-5 [%]	N-Q [%]	N-X [%]	P-1 [%]	O-1 [%]	O-2 [%]
Sample	N	P	O	398.0 eV	399.7 eV	400.8 eV	402.5 eV	133 eV	531.0 eV	532.0 eV
H_3PO_4/C-400	3.87	1.96	13.33	19.4	41.3	26.3	13	100	9.4	90.6
H_3PO_4/C-500	3.34	1.77	13.11	7.1	47.4	42.6	2.9	100	8.4	91.6
H_3PO_4/C-600	2.91	1.58	12.18	15.9	72.7	9.54	1.86	100	5.8	94.2
C-500	3.44	–	15.13	71.8	13.7	8.51	5.99	–	9.8	90.2

N (N-Q at 400.8 eV) and oxidized N (N-X at 400.5 eV) [27–30]. As shown in Table 1, it is clearly seen that H_3PO_4/C-500 contains 42.6% of N-Q functionality, much higher than 8.51% of C-500. The phosphorus bonded to nitrogen is reflected by the peaks at 398 and 400.8 eV that correspond P=N and P–N bonds, respectively [31]. For phosphorous, peak at 133.0 eV is attributed to phosphate and/or pyrophosphate groups (Fig. 3c) [29]. Oxygen is commonly presented in carbon as a consequence of its incorporation in the dangling bonds, as shown in Fig. 3b. Peaks at 531.0 eV (O-1) and 532.0 eV (O-2) are identified to C=O groups (carbonyl/quinone) and carbonyl oxygen atoms (phenol/ether), respectively [29]. Taking into account the presence of phosphorus in all carbons in this case, O-1 and O-2 entities also cover the contributions from non-bridging oxygen bonded to phosphorus P=O and bridging oxygen C–O–P [31]. It is also observed that the quantity of O-2 (>90%) is much larger than that of O-1 (<10%), which indicates the much contribution from bridging oxygen C-O-P. It is believed that N, P and O species in PCs are responsible for their pesudocapacitance.

The porosities of the obtained PCs were characterized by N_2 adsorption technique (Fig. 4a) and their pore size distributions are shown in Fig. 4b**.** Detailed information on the BET surface area (S_{BET}) and pore size distributions of all samples are summarized in Table 2. H_3PO_4/C-400 sample shows a low S_{BET} of 38.26 $m^2 g^{-1}$ and a small volume of 0.034 $cm^3 g^{-1}$ after H_3PO_4 activation at 400 °C. Significant increases are observed in both surface area and pore volume for H_3PO_4/C-500 and H_3PO_4/C-600 samples after the activation temperature increases to 500 and 600 °C, respectively. S_{BET} reaches 725.6 and 774.0 $m^2 g^{-1}$ as well as the pore volume gets to 0.446 and 0.451 $cm^3 g^{-1}$ for H_3PO_4/C-500 and H_3PO_4/C-600, respectively. Besides, nitrogen isotherms of H_3PO_4/C-500 and H_3PO_4/C-600 samples show a combined characteristic of I/IV types (Fig. 4a), indicating the presence of micro/mesoporous structures generated by *in situ* H_3PO_4 activation. As shown in Fig. 4b, the pore sizes of the resultant samples are centered at 1.0∼4.4 nm. Such porous structures are required for rapid ion transport, thus further improve the power characteristic of the supercapacitors [28,30]. For comparison, C-500 in the absence of H_3PO_4 shows a moderate S_{BET} of 156.4 $m^2 g^{-1}$, a small pore volume of 0.156 $cm^3 g^{-1}$ and a large pore size distribution at 2.0∼28 nm. Such results indicate H_3PO_4 plays an important role on the creation of microporous structures in the resultant carbon at high temperature.

N, O, P functionalities and porous structures of shrimp shell-derived carbons are valuable for supercapacitors. The electrochemical measurements of the resultant carbons were performed in 6 M KOH electrolyte using three-electrode cells. Fig. 5a shows

Table 2
Porous properties of different treated carbons from shrimp shell.

Sample	S_{BET} (m^2/g)	V_{total}[a] (cm^3/g)	Pore size (nm)
H_3PO_4/C-400	38.26	0.030	2.1∼3.9
H_3PO_4/C-500	725.6	0.446	1.0∼4.4
H_3PO_4/C-600	774.0	0.451	1.0∼4.4
C-500	156.4	0.156	2.0∼28

[a] The total pore volume for pores with diameter less than 162 nm at $P/P_0 = 0.994$.

the cyclic voltammetry (CV) curves of the obtained carbons at a scan rate of 10 mV s^{-1}. The CV curve of C-500 sample shows a completely distorted rectangular shape. With the increasing calcination temperature from 400 to 600 °C, the shape of CV curves is greatly improved, among which H_3PO_4/C-500 displays a nearly rectangular shape. It is observed that the areas enclosed by the CV curves are clearly different, indicating that capacitance decreases in the following order: H_3PO_4/C-500>H_3PO_4/C-600>H_3PO_4/C-400>C-500. Such obvious changes on the CV curves are probably attributed to their porous structures and doped heteroatoms in the carbons [31]. The galvanostatic charge/discharge curves at a current density of 100 mA g^{-1} are used to characterize the capacitive properties of the carbons, as shown in Fig. 5b. H_3PO_4/C-400 with low specific surface area and low content of N-Q exhibits the lowest electrochemical capacitance, while H_3PO_4/C-500 and H_3PO_4/C-600 show better linear characteristics than H_3PO_4/C-400. Such results agree with the description of CV curves. Fig. 5c gives the relationships between specific capacitance (Cs) and current density according to the galvanostatic charge and discharge results. The value of Cs is calculated according to $Cs = I \times \Delta t/(\Delta V \times m)$ from the discharge curves, where I is the constant discharge current, Δt is the discharge time, ΔV is the potential drop during discharge time, and m is the total mass of the active electrode materials [32]. The charge storage capacities of the obtained samples decrease in the following order: H_3PO_4/C-500>H_3PO_4/C-600>H_3PO_4/C-400>C-500. Such performances are in agreement with the character of the porous structures of those carbons, where the larger the specific surface area is, the higher the charge storage capacity is. However, C-500 sample shows the smallest Cs in all samples, though it has the larger surface area and O content than those of H_3PO_4/C-400. The low capacitance of C-500 may be attributed to its negative characters such as the wide pore size distribution (2.0∼28 nm), low N content (3.44%) and low N-Q percentage (8.51%). As previously reports, the micropores (<2 nm) are the most effective in a double-layer formation, and N groups (especially N-Q group) help in electron transfer through the

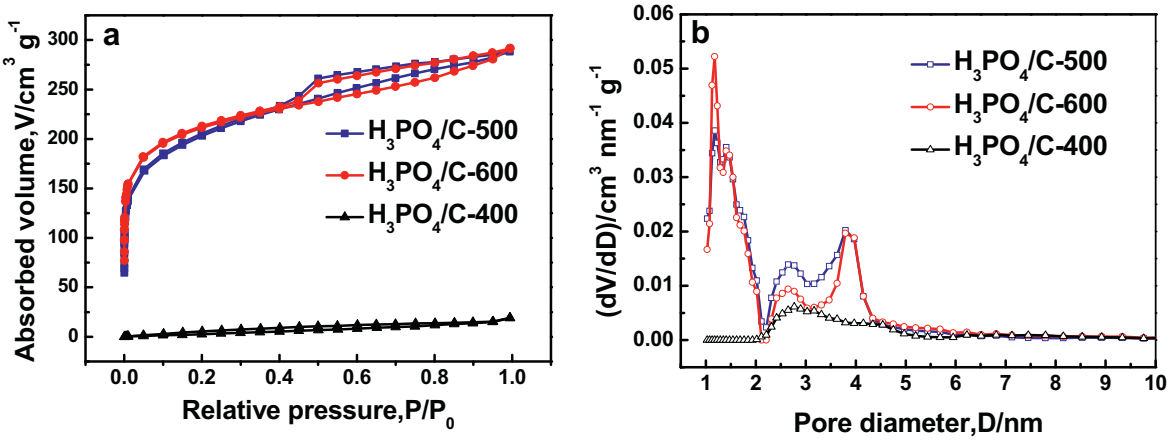

Fig. 4. (a) Nitrogen adsorption and desorption isotherms and (b) pore size distribution of H_3PO_4/C-400, H_3PO_4/C-500 and H_3PO_4/C-600 samples.

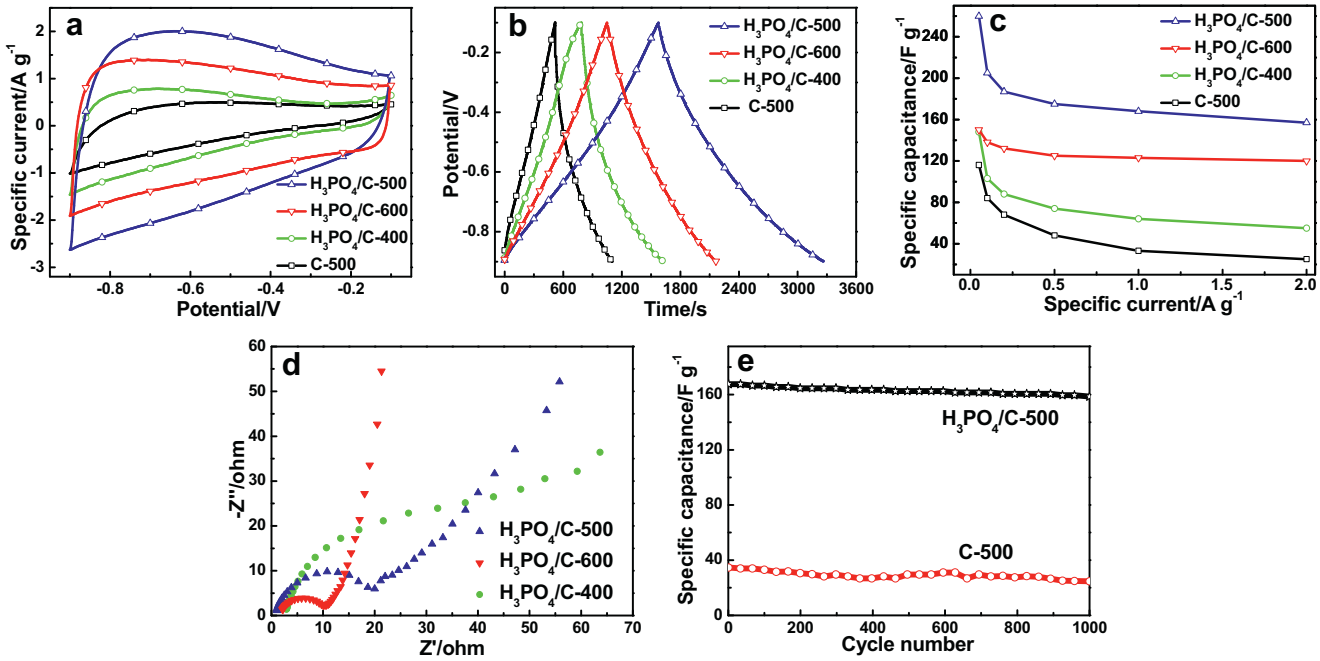

Fig. 5. Electrochemical characterizations of H_3PO_4/C composites in 6 M KOH solution at atmosphere temperature: (a) cyclic voltammograms (CV) at a scan rate of 10 mV s^{-1}; (b) charge-discharge cures at 100 mA g^{-1}; (c) specific capacitances at different current densities; (d) Nyquist plots of H_3PO_4/C-400, H_3PO_4/C-500 and H_3PO_4/C-600; (e) cycling performance of H_3PO_4/C-500 and C-500 for 1000th cycles loaded at a current density of 1 A g^{-1}.

carbon to increase the pseudocapacitive interactions [22,28,33]. H_3PO_4/C-500 presents the highest performance for 260, 206, 187, 175, 169 and 156 F g^{-1} at the current density of 0.05, 0.1, 0.2, 0.5, 1.0 and 2.0 A g^{-1}, respectively. The highest Cs is observed for H_3PO_4/C-500 in all samples at the tested range of current density, supporting results of the CV measurements. The improvement on capacitance is attributed to the synergetic effect of heteroatom surface properties and its porous structure. Firstly, H_3PO_4/C-500 sample with moderate N, O and P functionalities can enhance the wettability of the electrode [34]. The electronic structure of the N/O/P-containing functional groups and the conjugation of the p-electrons maybe provide reversible Faradic reaction sites for pseudocapacitance in spite of the unclear mechanism in basic electrolyte [30,34]. Furthermore, the formation of phosphorus-nitrogen accompanied with the decrease in bridging oxygen increases the heterogeneity of the carbon surface and results in compounds which have positive effects on the overall capacitance and on the improvement of the capacitance retention ratio [31]. The P species also benefit the improvement of the energy density for the supercapacitors, which will be discussed in the following two-electrode cells (Fig. 6). Secondly, the porosity of the material and its surface area are accessible for the species taking part in the electrochemistry sensitive process. The large surface area and pore volume help to significantly increase the electrostatic adsorption of electrolyte ions for energy storage in the EDLC.

Electrochemical impedance spectroscopy (EIS) provides complementary information to further understand their capacitive behaviors, as shown in Fig. 5d. Nyquist plots of H_3PO_4 activated carbons at different temperatures exhibit two distinct parts, including a semicircle in the high frequency region and a slope line in the low frequency region. It is reported that a larger diameter of semicircle for the electrode reflects the existence of higher R_{ct} (charge-transfer resistance) in the high frequency region, indicating the rich N, O-containing functional groups in samples [35]. It is obvious that R_{ct} is the following order: H_3PO_4/C-400>H_3PO_4/C-500>H_3PO_4/C-600, which is attributed to their different contents of nitrogen and oxygen as demonstrated in Table 1. Similarly, the deviation in slope at the very low frequencies might derive from the contribution of pseudocapacitance, in accordance with their N, O-doping nature [36]. The EIS

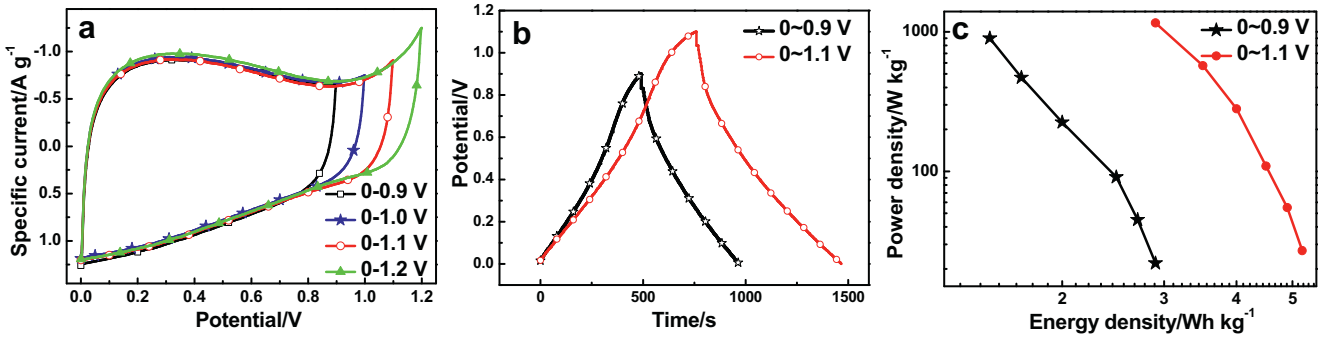

Fig. 6. (a) CV curves of H_3PO_4/C-500 at a scan rate of 5 mV s^{-1} (two-electrode cell) based on different cell voltages of 0.9, 1.0, 1.1 and 1.2 V in 6 M KOH; (b) The charge-discharge curves of H_3PO_4/C-500 sample at the cell voltages of 0.9 and 1.1 V (50 mA g^{-1}); (c) Ragone plots of H_3PO_4/C-500 at 0.9 and 1.1 V.

results further support the previous results of the CV curves and charge/discharge profiles shown in Figs. 5a–c.

The stability of the capacitance performance of H_3PO_4/C-500 and C-500 was evaluated by 1000 cycles at a current density of 1 A g^{-1} (Fig. 5e). The *Cs* of C-500 electrode is found to gradually decrease in the last 400 cycles, resulting in a capacitance retention of about 71.3% after the 1000 continuous cycles. While the *Cs* of H_3PO_4/C-500 electrode slightly drops 6.0% from 168 to 158 F g^{-1}, still more than 94.0% in the whole cycles, demonstrating the long-term stability of H_3PO_4/C-500 as electrode material. Such improved stability and high capacitance can be related to the co-existence of mesopores with micropors in H_3PO_4/C-500.

The energy density of supercapacitors is codetermined by specific capacitance operation voltage. The capacitive behaviors of H_3PO_4/C-500 sample are also examined in two cell system, and the results are shown in Fig. 6. A large electrochemical potential window up to 1.1 V can be achieved, as seen in Figs. 6a–b. H_3PO_4/C-500 demonstrates stable electrochemical performance even at high cell voltage up to 1.1 V, which is close to the theoretical decomposition potential of water (1.23 V). However, the electrolyte decomposition peak seems to appear at a cell voltage of 1.2 V. The widening of operation voltage window is due to the blockage of the electrochemical active oxidation sites of H_3PO_4/C-500 by phosphorus groups (see supporting information S1). The result is similar to the reported work in literature [14,26]. Thus, widening the operating voltage up to 1.1 V can significantly increase the energy density of the devices compared with that of 0.9 V. Ragone plots of H_3PO_4/C-500 obtained at 0.9 and 1.1 V are shown in Fig. 6c. The specific energy density of H_3PO_4/C-500 in two-electrode cell is 2.9 W h kg^{-1} at 0.9 V and can increase to 5.2 W h kg^{-1} at 1.1 V, whereas the specific power density increases from 914 to 1162 W kg^{-1}, respectively. The results show that H_3PO_4 activation is a good technique to obtained P-doped PCs with increased energy and power densities, which agrees with the reported work [37].

4. Conclusions

N, O, P heteroatom decorated PCs for supercapacitors have been successfully prepared by one step H_3PO_4 activation of shrimp shell. The contents of N, O and P functional groups in the resultant PCs along with their porosities are temperature-dependent. PCs with abundant pores and heteroatom functionalities are good electrode materials for supercapacitors. N, O, P decorated PCs with suitable porous structure exhibit good capacitive behaviors, including large capacitance, long cycle life, high energy and power densities. Benefited from above advantages and the low cost shrimp shell as precursor, the prepared PCs have attractive application future for supercapacitors.

Acknowledgements

This work is supported by the NSFC (Nos. 51372277, 50902066), China Postdoctoral Science Foundation (2013M530922, 2014T70253) and Program for Liaoning Excellent Talents in University (LJQ2014118) and the Fundamental Research Funds for the Central Universities (No.15CX08005A).

Appendix A. Supplementary data

Supplementary data associated with this article can be found, in the online version, at http://dx.doi.org/10.1016/j.electacta.2015.07.094.

References

[1] Y. Zhai, Y. Dou, D. Zhao, P.F. Fulvio, R.T. Mayes, S. Dai, Carbon materials for chemical capacitive energy storage, Adv Mater 23 (2011) 4828.
[2] Y.B. Xie, X.Q. Fang, Electrochemical flexible supercapacitor based on manganese dioxide-titanium nitride nanotube hybrid, Electrochim. Acta 120 (2014) 273.
[3] M.R. Lukatskaya, O. Mashtalir, C.E. Ren, Y. Dall, P. Rozier, P.L. Taberna, M. Naguib, P. Simon, M.W. Barsoum, Y. Gogotsi, Cation intercalation and high volumetric capacitance of two-dimensional titanium carbide, Science 341 (2013) 1502.
[4] H. Wang, H. Dai, Strongly coupled inorganic-nano-carbon hybrid materials for energy storage, Chem. Soc. Rev. 42 (2013) 3088.
[5] Y.W. Zhu, S. Murali, M.D. Stoller, K.J. Ganesh, W.W. Cai, P.J. Ferreira, A. Pirkle, R. M. Wallace, K.A. Cychosz, M. Thommes, D. Su, E.A. Stach, R.S. Ruoff, Carbon-based supercapacitors produced by activation of graphene, Science 332 (2011) 1537.
[6] S. Uppugalla, U. Male, P. Srinivasan, Design and synthesis of heteroatoms doped carbon/polyaniline hybrid material for high performance electrode in supercapacitor application, Electrochim. Acta 146 (2014) 242.
[7] J. Chmiola, C. Largeot, P.L. Taberna, P. Simon, Y. Gogotsi, Desolvation of ions in subnanometer pores and its effect on capacitance and double-layer theory, Angew. Chem. Int. Ed. 47 (2008) 3392.
[8] K. Xie, X. Qin, X. Wang, Y. Wang, H. Tao, Q. Wu, L. Yang, Z. Hu, Carbon nanocages as supercapacitor electrode materials, Adv Mater 24 (2012) 347.
[9] C. Liu, F. Li, L.P. Ma, H.M. Cheng, Advanced materials for energy storage, Adv Mater. 22 (2010) E28.
[10] P. Simon, Y. Gogotsi, Materials for electrochemical capacitors, Nat. Mater 7 (2008) 845.
[11] G. Otrokhov, D. Pankratov, G. Shumakovich, M. Khlupova, Y. Zeifman, I. Vasil'eva, O. Morozova, A. Yaropolov, Enzymatic synthesis of polyaniline/multi-walled carbon nanotube composite with core shell structure and its electrochemical characterization for supercapacitor application, Electrochim. Acta 123 (2014) 151.
[12] Y. Tan, C. Xu, G. Chen, Z. Liu, M. Ma, Q. Xie, N. Zheng, S. Yao, Synthesis of ultrathin nitrogen-doped graphitic carbon nanocages as advanced electrode materials for supercapacitor, ACS Appl. Mater. Interfaces 5 (2013) 2241.
[13] X. He, P. Ling, J. Qiu, M. Yu, X. Zhang, C. Yu, M. Zheng, Efficient preparation of biomass-based mesoporous carbons for supercapacitors with both high energy density and high power density, J. Power Sources 240 (2013) 109.
[14] U.B. Nasini, V.G. Bairi, S.K. Ramasahayam, S.E. Bourdo, T. Viswanathan, A.U. Shaikh, Phosphorous and nitrogen dual heteroatom doped mesoporous carbon synthesized via microwave method for supercapacitor application, J. Power Sources 250 (2014) 257.
[15] H. Zhu, J. Yin, X.L. Wang, H.Y. Wang, X.R. Yang, Microorganism-derived heteroatom-doped carbon materials for oxygen reduction and supercapacitors, Adv. Funct. Mater. 23 (2013) 1305.
[16] W. Shen, W. Fan, Nitrogen-containing porous carbons: synthesis and application, J. Mater. Chem. A 1 (2013) 999.
[17] N.D. Kim, S.J. Kim, G.P. Kim, I. Nam, H.J. Yun, P. Kim, J. Yi, NH3-activated polyaniline for use as a high performance electrode material in supercapacitors, Electrochim. Acta 78 (2012) 340.
[18] L. Wei, M. Sevilla, A.B. Fuertes, R. Mokaya, G. Yushin, Hydrothermal carbonization of abundant renewable natural organic chemicals for high-performance supercapacitor electrodes, Adv. Energy Mater. 1 (2011) 356.
[19] L. Zhao, L.Z. Fan, M.Q. Zhou, H. Guan, S.Y. Qiao, M. Antonietti, M.M. Titirici, Nitrogen-containing hydrothermal carbons with superior performance in supercapacitors, Adv. Mater. 22 (2010) 5202.
[20] Z. Li, Z.W. Xu, X.H. Tan, H.L. Wang, C.M.B. Holt, T. Stephenson, B.C. Olsen, D. Mitlin, Mesoporous nitrogen-rich carbons derived from protein for ultra-high capacity battery anodes and supercapacitors, Energy Environ. Sci. 6 (2013) 871.
[21] R.J. White, M. Antonietti, M.M. Titirici, Naturally inspired nitrogen doped porous carbon, J. Mater. Chem. 19 (2009) 8645.
[22] F. Su, C.K. Poh, J.S. Chen, G. Xu, D. Wang, Q. Li, J. Lin, X.W. Lou, Nitrogen-containing microporous carbon nanospheres with improved capacitive properties, Energy Environ. Sci. 4 (2011) 717.
[23] Z. Lei, N. Christov, L.L. Zhang, X.S. Zhao, Mesoporous carbon nanospheres with an excellent electrocapacitive performance, J. Mater. Chem. 21 (2011) 2274.
[24] S.J. Parikh, J. Chorover, ATR-FTIR spectroscopy reveals bond formation during bacterial adhesion to iron oxide, Langmuir 22 (2006) 8492.
[25] C.B. Cao, H. Wang, H. Zhu, Carbon nitride films deposited from organic solutions by electrodeposition, Diamond Relat. Mate. 9 (2000) 1786.
[26] X. Fan, C. Yu, Z. Ling, J. Yang, J. Qiu, Hydrothermal synthesis of phosphate-functionalized carbon nanotube-containing carbon composites for supercapacitors with highly stable performance, ACS Appl. Mater. Interfaces 5 (2013) 2104.
[27] Y. Li, Y. Zhao, H.H. Cheng, Y. Hu, G.Q. Shi, L.M. Dai, L.T. Qu, Nitrogen-doped graphene quantum dots with oxygen-rich functional groups, J. Am. Chem. Soc. 134 (2012) 15.
[28] D. Hulicova-Jurcakova, M. Seredych, G.Q. Lu, T.J. Bandosz, Combined effect of nitrogen- and oxygen-containing functional groups of microporous activated

carbon on its electrochemical performance in supercapacitors, Adv. Funct. Mater. 19 (2009) 438.
[29] C. Wang, L. Sun, Y. Zhou, P. Wan, X. Zhang, J. Qiu, P/N co-doped microporous carbons from H3PO4-doped polyaniline by in situ activation for supercapacitors, Carbon 59 (2013) 537.
[30] X.Y. Chen, C. Chen, Z.J. Zhang, D.H. Xie, X. Deng, J.W. Liu, Nitrogen-doped porous carbon for supercapacitor with long-term electrochemical stability, J. Power Sources 230 (2013) 50.
[31] D. Hulicova-Jurcakova, M. Seredych, G.Q. Lu, N.K.A.C. Kodiweerac, P.E. Stallworth, S. Greenbaum, T.J. Bandosz, Effect of surface phosphorus functionalities of activated carbons containing oxygen and nitrogen on electrochemical capacitance, carbon 47 (2009) 1576.
[32] J.Y. Qu, F. Gao, Q. Zhou, Z.Y. Wang, H. Hu, B.B. Li, W.B. Wan, X.Z. Wang, J.S. Qiu, Highly atom-economic synthesis of graphene/Mn3O4 hybrid composites for electrochemical supercapacitors, Nanoscale 5 (2013) 2999.
[33] M. Wu, P. Ai, Mi. Tan, B. Jiang, Y. Li, J. Zheng, W. Wu, Z. Li, Q. Zhang, X. He, Synthesis of starch-derived mesoporous carbon for electric double layer capacitor, Chem. Eng. J. 245 (2014) 166.
[34] S.L. Candelaria, B.B. Garcia, D. Liu, G. Cao, Nitrogen modification of highly porous carbon for improved supercapacitor performance, J. Mater. Chem. 22 (2012) 9884.
[35] Z.B. Lei, L. Lu, X.S. Zhao, The electrocapacitive properties of graphene oxide reduced by urea, Energy Environ. Sci. 5 (2012) 6391.
[36] H. Zhu, X. Wang, X. Liu, X. Yang, Integrated synthesis of poly (o-phenylenediamine)-derived carbon materials for high performance supercapacitors, Adv Mater. 24 (2012) 6524.
[37] J.P. Paraknowitsch, A. Thomas, Doping carbons beyond nitrogen: an overview of advanced heteroatom doped carbons with boron, sulphur and phosphorus for energy applications, Energy Environ. Sci. 6 (2013) 2839.